

Revision 1

Synchrotron Mössbauer study of Fe-bearing pyrope at high pressures and temperatures

Zhu Mao[1], Jung-Fu Lin[1], Shu Huang[2], Jiuhua Chen[2], Yuming Xiao[3], Paul Chow[3]

[1]Department of Geological Sciences, Jackson School of Geosciences, The University of Texas at Austin, Austin, TX 78712, USA

[2]Department of Mechanical and Materials Engineering, Florida International University, Miami, FL 33172, USA

[3]HPCAT, Carnegie Institution of Washington, Advanced Photon Source, Argonne National Laboratory, Argonne, IL 60439, USA

ABSTRACT

Iron-bearing pyrope, an abundant silicate mineral in the Earth's upper mantle, exhibits the largest quadrupole splitting (QS) in Mössbauer spectrea among all common Fe-bearing rock-forming silicate minerals at ambient conditions, with a value of approximately 3.5 mm/s. Knowledge regarding the hyperfine QS of the mantle minerals at relevant pressures and temperatures (P-T) is increasingly needed to aid our understanding of the electronic spin and valence states of iron and local site distortion in major mantle silicate minerals. Here we have measured synchrotron Mössbauer spectra (SMS) of the high-spin Fe^{2+} in Fe-bearing pyrope garnet with two distinct compositions, $(Mg_{0.8}Fe_{0.2})_3Al_2Si_3O_{12}$ (py80alm20) and $Fe_3Al_2Si_3O_{12}$ (alm100), up to 30 GPa and 750 K. Analyses of the SMS spectra revealed that the high-spin Fe^{2+} ions in the distorted dodecahedral site exhibit extremely high QS of ~3.4-3.6 mm/s and relatively high chemical shifts (CS) of ~1.2-1.3 mm/s at high P-T, indicating that the Fe^{2+} ions remains in the high-spin state. An increase in the Fe content in the pyrope-almandine series only slightly decreases the QS and CS of the Fe^{2+} ions. To decipher the energy separation (Δ) between the two lowest energy levels of the 3*d* electrons of the Fe^{2+} ions in the sample, the d_{xy} and d_z^2 orbitals, the QS values of py80alm20 at high P-T were further evaluated using Huggins model. Our modeled results show that the Δ of the Fe^{2+} ions in py80alm20 is approximately 156 meV at high P-T, and may be correlated to the change of the crystal-field energy splitting (Δ_C). Comparison of the QS, Δ, and Δ_C values of Fe^{2+} ions in the distorted dodecahedral sites of pyrope and silicate perovskite indicates that the high-spin Fe^{2+} with the extremely high QS can remain stable at high P-T conditions, consistent with recent theoretical predictions. Our results thus contribute to our current understanding of the hyperfine parameters and spin and valence states of iron in the mantle silicate minerals at high P-T.

Keywords: Fe-bearing Pyrope, Mössbauer Spectroscopy, High Pressure, High Temperature, Hyperfine Parameters

INTRODUCTION

Iron-bearing pyrope is one of the major constituents in the Earth's crust and upper mantle, and is commonly found in many igneous and metamorphic rocks (e.g. Deer et al. 1982; Ringwood 1991). The pyrope ($Mg_3Al_2Si_3O_{12}$; abbreviated as py) - almandine ($Fe_3Al_2Si_3O_{12}$; abbreviated as alm) solid solution represents the dominant garnet composition and is thus of great geological and petrological interest. Fe-bearing pyrope crystallizes in the cubic system with a space group *Ia3d* in which the divalent Mg^{2+} and Fe^{2+} cations occupy the large eight-fold dodecahedral sites, while the Al^{3+} and Si^{4+} cations are located in the center of the six-fold octahedral and four-fold tetrahedral sites, respectively (Zemann and Zemann 1961; Gibbs and Smith 1965). Due to its geological abundance, physical properties of pyrope-almandine have attracted extensive research interest, including the study of their crystal structure (e.g. Gibbs and Smith 1965; Armbruster et al. 1992), elasticity (e.g. Chai et al. 1997; Conrad et al. 1999; Sinogeikin and Bass 2000; Jiang et al. 2004), and thermodynamics (e.g. Haselton and Westrum 1980; Wang et al. 2000).

The particularity of the Fe-bearing pyrope in mineral physics pertains to the extremely high quadrupole splitting (QS) of 3.47-3.58 mm/s observed in Mössbauer spectra at ambient conditions. This is, in fact, the largest QS ever observed among all common Fe-bearing silicate minerals under ambient environments (e.g. Bancroft et al. 1967; Lyubutin and Dodokin 1970; Huggins 1975; Amthauer et al. 1976; Murad and Wagner 1987; Geiger et al. 1992; Černá et al. 2000). As measured by Mössbauer spectroscopy (MS), the QS represents the splitting of the nuclear energy levels caused by the interaction of the nuclear quadrupole moment with the electric field gradient (EFG) (Dyar et al. 2006). The QS value is governed by the iron electronic state and its local surrounding in the crystal lattice. It depends on the pressure-temperature (P-T), crystal-field splitting, and valence and spin states of Fe in minerals. The QS value also reflects the degree of the lattice distortion for the coordination polyhedron surrounding the Fe atoms (Burns and Solberg

1988). The largest QS in Fe-bearing pyrope thus indicates an extremely high lattice distortion of the dodecahedral Fe^{2+} site.

Data on the hyperfine QS values of minerals at a given P-T condition provide necessary constraints on the crystal-field splitting parameters (Fig. 1) (e.g. Huggins 1975; Lin et al. 2009) that are essential for understanding the electronic spin and valence states in mantle minerals. For Fe-bearing pyrope, the five 3*d* energy levels, together with the crystal-field stabilization energy (Δ_C), have been determined using optical absorption and Mössbauer spectroscopic methods at ambient P-T (Fig. 1) (White and Moore 1972; Huggins 1975). On the other hand, Lin et al. (2009) have measured the QS of lower-mantle ferropericlase ($(Mg_{0.75}Fe_{0.25})O$) at high P-T to determine the crystal-field splitting energy of the lowest level (Δ) in the octahedral Fe^{2+} site using synchrotron Mössbauer spectroscopy (SMS) in an externally-heated diamond anvil cell (EHDAC) (Fig. 1). At a given pressure, the QS of Fe^{2+} as a function of temperature follows the Boltzmann distribution with Δ (Huggins 1975). The observed increase in Δ with pressure directly correlates with the variation of the spin crossover in ferropericlase at high P-T (Fig. 1) (Lin et al. 2009). In addition, recent experimental studies revealed that Fe^{2+} in Fe-bearing silicate perovskite ($(Mg,Fe)SiO_3$), the most abundant mineral phase in the Earth's lower mantle, exhibits extremely high QS (as high as ~4.4 mm/s) at above approximately 30 GPa (Lin et al. 2008, 2012; McCammon et al. 2008, 2010; Narygina et al. 2010). Fe^{2+} in perovskite occupies the pseudo-dodecahedral site (A-site) that is similar to the distorted dodecahedral site in Fe-bearing pyrope (Fig. 1). Combined with previous XES analyses for the total spin momentum of iron in perovskite (Badro et al. 2004; Li et al. 2006), the extremely high QS of Fe^{2+} in the A-site has been interpreted as an occurrence of the intermediate-spin Fe^{2+} with a total spin momentum of one (S=1) at above 30 GPa (McCammon et al. 2008, 2010; Narygina et al. 2010). First-principle theoretical calculations, on the other hand, show that the high-spin Fe^{2+} in the A site is much more stable than the intermediate-spin state at lower-mantle pressures (Zhang et al. 2006; Stackhouse et al. 2007; Bengtson et al. 2009; Caracas et al. 2010; Hsu et al. 2010, 2011; Umemoto et al. 2010), and the extremely high QS site is interpreted as a result of a change of the position of iron which moves away from the central positions in the A site at high pressures (Bengtson et al. 2009; Hsu et al. 2010, 2011). We note that the occurrence of the intermediate-spin state in geological materials is very rare in literature reports (e.g., Dyar et al. 2006). In addition, Fe^{2+} in silicate post-perovskite ($(MgFe)SiO_3$) also displays extremely high QS at lowermost mantle pressures (Lin et al. 2008; Mao et al. 2010; Yu et al. 2012).

Considering the similarity in the crystallographic environments and the magnitude of the QS of Fe^{2+} on Fe-bearing pyrope, perovskite, and post-perovskite, experimental studies on the local electronic structures and hyperfine parameters of Fe-bearing pyrope as a function of P-T can provide new insights into the spin states of Fe^{2+} in the lower-mantle minerals. The QS and chemical shift (CS) of Fe-bearing pyrope have only been determined by Mössbauer spectroscopy at temperatures up to 800 K under ambient pressure in previous studies (Bancroft et al. 1967; Lyubutin and Dodokin 1970; Prandle 1971; Huggins 1975; Amthauer et al. 1976; Murad and Wagner 1987; Geiger et al. 1992; Černá et al. 2000). The combined effects of P-T on these parameters remain largely unknown, significantly limiting our understanding on the electronic structures of Fe-bearing pyrope and other major rock-forming silicates at high P-T. In this study, we have measured and analyzed SMS spectra of two Fe-bearing pyropes at P-T conditions relevant to the Earth's upper mantle. The derived QS values of the Fe-bearing pyrope at high P-T were used to constrain the energy splitting between the two-lowest d_{xy} and d_{z^2} orbitals and to help understand the local electronic environments of Fe^{2+} at the dodecahedral site.

EXPERIMENTAL DETAILS

Two single-crystal Fe-bearing pyropes, py80alm20 [$(Mg_{0.8}Fe_{0.2})_3Al_2Si_3O_{12}$] and alm100 [$Fe_3Al_2Si_3O_{12}$], were synthesized from ^{57}Fe-enriched starting glasses. Mixed oxides, $^{57}Fe_2O_3$+^{57}Fe+Al_2O_3+SiO_2 (>95% enrichment) and MgO+Al_2O_3+SiO_2, were weighted for $Mg_3Al_2Si_3O_{12}$ and $Fe_3Al_2Si_3O_{12}$ composition, respectively, and then melted in a plasma melting device to produce pyrope-like glass and almandine-like glass. The $Fe_3Al_2Si_3O_{12}$ glass was then loaded in a 14/8 cell multi-anvil cell assembly and heated to 1223 K at 2.5 GPa for 24 hours to synthesize alm100 single crystals. To synthesize single-crystal py80alm20, we mixed 80 mol.% pyrope-like glass with 20 mol.% almandine-like glass. The glass mixture was heated to 1523 K at 2.8 GPa for 20 hours in the multi-anvil cell. The synthesized py80alm20 and alm100 crystals were examined by X-ray diffraction and electron microprobe analyses to confirm the crystal structure and chemical compositions, respectively. The py80alm20 and alm100 single crystals were polished to ~20 μm in thickness. For high-pressure measurements at 300 K, the py80alm20 and alm100 crystals were loaded into symmetric diamond anvil cells (DACs) with Re gasket and Ne pressure medium. Ruby spheres close to the samples served as a pressure calibrant (Mao et al. 1986). For the high P-T experiments on py80alm20, the sample was loaded with Ne in an

EHDAC. A K-type thermocouple for temperature measurements was attached to the surface of one of the two diamond anvils, approximately 500 μm away from its culet. Pressures were determined from the fluorescence shift of the ruby spheres by taking temperature effects into account (Rekhi et al. 1999).

SMS experiments were conducted at HPCAT sector of the Advanced Photon Source (APS), Argonne National Laboratory (ANL). The ^{57}Fe nuclei in the sample were excited by an X-ray beam with an energy of 14.4125 keV and a bandwidth of approximately 2 meV. The SMS spectra were recorded by an avalanche photodiode detector in the forward direction with a collection time of approximately one hour for each spectrum. SMS spectra of the py80alm20 and alm100 samples were collected with or without a stainless steel foil in a pressure step of 3-4 GPa up to 30 GPa at 300 K. The stainless steel foil was used as the reference to determine the CS of the Fe^{2+} in the samples. To constrain the temperature effect on the hyperfine parameters, Mössbauer spectra of py80alm20 were also collected at temperatures up to 750 K and pressures up to 25 GPa in an EHDAC.

RESULTS

SMS spectra of py80alm20 and alm100 are dominated by five quantum beats in the time window up to 125 ns at the investigated P-T range, immediately indicating the high QS value of the Fe-bearing pyrope (Fig. 2). Increasing pressure at 300 K only has a small effect on the QS by slightly moving the position of five time beats toward faster time decay. In contrast to the effect of pressure, elevating temperature at a given pressure weakly causes the five time beats of Fe-bearing pyrope to move toward slower time decay (Fig. 2).

Mössbauer spectra of the Fe-bearing pyropes were analyzed using the CONUSS program (Fig. 2) (Sturhahn 2000). The obtained SMS spectra were evaluated with a single-doublet model with Fe^{2+} in the dodecahedral site (e.g. Lyubutin and Dodokin 1970; Geiger et al. 1992). The QS values of both samples increased by 1% with pressure up to 2 GPa, but only showed weak pressure dependence above 2 GPa (Fig. 3). At a given temperature, the CS values decreased linearly with pressure up to 30 GPa for both samples (Fig. 3); the pressure derivative of the CS is approximately -0.0020 (±0.0004) mm/(s·GPa) for each sample. High P-T experiments show that elevating temperature at a given pressure leads to the decrease of the QS and CS of py80alm20 (Fig. 4), consistent with previous experimental results (Lyubutin and Dodokin 1970). The temperature effect on the QS weakens with increasing pressure, while the effect of temperature on the CS is similar at all investigated pressures. The temperature derivative of the CS for py80alm20 is approximately -3.2×10^{-4} ($\pm0.2\times10^{-4}$) mm/(s·K).

DISCUSSION

Fe-bearing pyrope exhibits the largest QS of any known Fe-bearing silicates and oxides of geological relevance at ambient conditions (e.g. Bancroft et al. 1967; Dodokin et al. 1973). Our SMS results further show that the QS values of py80alm20 remain extremely high at high P-T conditions relevant to the upper mantle. Increasing the Fe content in the pyrope-almandine system slightly increases the QS and CS values (Fig. 3), consistent with previous experimental observations (e.g., Lyubutin and Dodokin 1970; Prandl 1971;

Amthauer et al. 1976; Murad and Wagner 1987; Černá et al. 2000). Overall, high P-T conditions have relatively weak effects on the QS of the system—the QS increases by approximately 1% from ambient pressure to 2 GPa and another 1% from 2 GPa to 30 GPa, respectively. The QS of py80alm20 decreases by 5-6 % with increasing temperature from 300 K to 750 K at high pressures (Fig. 4).

As noted earlier, knowledge concerning the hyperfine parameters at high P-T has served as one of the most effective means for understanding the spin and valence states of Fe^{2+} in mantle minerals. In particular, the splitting of the lowest-energy 3*d* orbital of minerals can be derived from the temperature-dependent QS values that can be determined from Mössbauer spectra (Ingalls 1964; Huggins 1975; Lin et al. 2009). Here the variation of the QS as a function of temperature at a given pressure for Fe^{2+} in the dodecahedral site in py80alm20 has been evaluated using Huggins model (Huggins 1975). The QS can be attributed to two major contributions, QS measured at 0 K (QS(0K)) and lattice contribution (QS_{latt}), and depends on the temperature and the separation of the two-lowest d_{xy} and d_{z^2} orbitals, Δ (Fig. 1). Based on Huggins model, the QS follows the Boltzmann distribution function with temperature and Δ:

$$QS(T) = (QS(0K) + QS_{latt})\frac{1-\exp(-\Delta/kT)}{1+\exp(-\Delta/kT)} - QS_{latt}, \quad (1)$$

where *k* is Boltzmann's constant. At a given pressure, QS(0K) and QS_{latt} are constants and do not change with temperature.

The QS_{latt} contribution has been mostly ignored in previous studies because of its much smaller value compared to the QS(0K) (Ingalls 1964; Lyubutin and Dodokin 1970;

Huggins 1975; Lin et al. 2009). However, the variation of QS_{latt} appears to be affected by the value of Δ. For instance, greatly varying the QS_{latt} of Fe-bearing pyrope by 1 mm/s (approximately 30% of QS) leads to a 100 cm^{-1} change in Δ (Huggins 1975). In particular, we have noted that the QS_{latt} contribution needs to be considered in properly modeling the QS of pyrope using the Boltzmann distribution function, indicating that the QS_{latt} contribution cannot be ignored for minerals with extremely high QS and lattice distortion, such as the case of pyrope. This differs from the ferropericlase case which has much smaller QS (~1 mm/s), and thus the QS_{latt} contribution has been ignored (Kantor et al. 2006; Lin et al. 2006, 2009). Modeling the QS values using both QS(0K) and QS_{latt} also allowed us to examine how the ratio of these contributions is affected by pressure. Our modeled results show that the derived QS_{latt} is of opposite sign to the QS(0K), consistent with theoretical predictions (Fig. 5) (Ingalls 1964), and is greatly enhanced by elevated pressure (Fig. 5). At 1 bar, the QS(0K) constitutes 76% of the total QS at 0 K while the QS_{latt} contribution accounts for 24% of the total QS, much less than the QS(0K) contribution. However, the ratio of the QS_{latt} contribution increases to 41% at 1.3 GPa, indicating a great drop in the QS(0K) contribution (Fig. 5), although further increase in pressure to 25 GPa has a minor effect on the QS_{latt} to QS(0K) ratio (Fig. 5). The ratio change can be associated with the initial increase in the QS of Fe-bearing pyrope below 2 GPa. Such increase in the QS_{latt} contribution may be attributed to an increased distortion of the Fe^{2+} dodecahedral site with the applied pressure initially, although it becomes less sensitive to pressure above 2 GPa.

Based on the temperature-dependent Boltzmann distribution model (equation (1)), we have also derived the energy separation of the two-lowest levels, Δ (Fig. 6), which is an important crystal-field parameter for understanding the electronic spin-pairing transitions of Fe in major mantle minerals. According to the crystal field theory (Burns 1993), the spin transition of Fe occurs when the crystal-field splitting energy, Δ_C, increases with pressure and eventually overcomes the spin-pairing energy. Previous resonant X-ray emission spectroscopic experiments confirmed this notion (Lin et al. 2010), showing an increase in the Δ_C of ferropericlase before the spin transition. However, optical absorption experiments (Keppler et al. 2007) observed a slight decrease in the Δ_C of ferropericlase before the transition. Most importantly, the increase of the Δ_C in ferropericlase with pressure is accompanied with an increase of Δ in the high P-T SMS study (Lin et al. 2009). Knowing the effect of pressure on Δ thus provides additional information on the spin state of Fe in mantle minerals.

The Δ of 1100 cm^{-1} for Fe-bearing pyrope is much greater than 290-770 cm^{-1} for ferropericlase at high pressures and higher than 500 cm^{-1} for silicate perovskite at ambient conditions (Figs. 1 and 6) (Keppler et al. 1994; Lin et al. 2009). The Δ of py80alm20 represents the energy difference between the d_{xy} and d_{z^2} orbitals of the e_g states of Fe^{2+} in the dodecahedral site (Fig. 1). Our derived Δ of py80alm20 is 195 meV at 1 bar, drops to 156 meV at 1.3 GPa, and then slightly decreases to 144 meV at 25 GPa (Fig. 6). That is, the Δ of py80alm20 has a weak dependence on pressure between 1.3 and 25 GPa. The decrease of the Δ with pressure indicates a lower-degree energy separation between the d_{xy} and d_{z^2} orbitals at high pressures. As noted above, the variation of Δ with pressure is positively correlated with the change of Δ_C with pressure for ferropericlase (Lin et al. 2009, 2010). To the best of our knowledge, there is no theoretical or experimental study discussing the correlation of Δ and Δ_C as a function of pressure, though it is conceivable that Δ and Δ_C follow a similar trend to that in ferropericlase with increasing pressure. In this case, increasing pressure should slightly lower the Δ_C of Fe^{2+} in the dodecahedral site, similar to the Δ of Fe-bearing pyrope observed here (Fig. 6).

The pressure-dependence of the Δ_C for Fe-bearing pyrope obtained in this study sheds new lights on understanding the electronic structures of Fe^{2+} in similar crystallographic sites, such as Fe^{2+} in the pseudo-dodecahedral site of silicate perovskite or even in post-perovskite (e.g. Hsu et al. 2010, 2011; Lin et al. 2008, 2012; Yu et al. 2012). Unlike ferropericlase, the electronic spin states of Fe^{2+} in silicate perovskite remain highly debated (e.g., Lin et al. 2008, 2011, 2012; McCammon et al. 2008; Narygina et all. 2009; Hsu et al. 2010, 2011). Previous SMS studies revealed that Fe^{2+} in silicate perovskite exhibits extremely high QS as high as ~4.4 mm/s at pressures above 30 GPa (Fig. 7) (Lin et al. 2008, 2012; McCammon et al. 2008; Mao et al. 2011), and the QS of Fe^{2+} in perovskite is only slightly affected by pressure above ~20 GPa (Lin et al. 2012), similar to the high QS values of Fe-bearing pyrope as a function of pressure. Owing to the similarity of the QS values and the Fe sites between Fe-bearing pyrope and perovskite, it is likely that the pressure-dependence of the Δ_C for perovskite is similar to that of Fe-bearing pyrope. Since the Δ_C of py80alm20 slightly decreases with pressure, it is conceivable that the Δ_C of perovskite will not be strongly affected by applied pressure at mantle pressures, indicating that the high-spin Fe^{2+} could remain stable at P-T conditions relevant to the lower mantle. Similar to Fe-bearing pyrope, the extremely high observed QS of perovskite could thus be a result of strong atomic site distortions (Hsu et al. 2010, 2011; Lin et al. 2012).

In conclusion, our high P-T SMS measurements provide direct means to understand the 3*d* electronic structures of Fe-bearing pyrope. A great value QS of Fe-bearing pyrope at both ambient and high P-T conditions reveals a significant atomic site distortion, rather than any change in the electronic spin state. Elevating pressure leads to a weak increase in the QS but a decrease in the CS, whereas increasing temperature lowers both QS and CS values. At a given pressure, fitting the QS values of Fe-bearing pyrope using the temperature-dependent Boltzmann distribution function, Huggins model, yields the energy splitting (Δ) of the d_{xy} and d_{z^2} orbitals. The slight decrease of the Δ with pressure in Fe-bearing pyrope may indicate a weak dependence of the crystal-field splitting energy (Δ_C) for Fe^{2+} in the dodecahedral site (e.g., Lin et al. 2009, 2010). Comparisons of the Δ and Δ_C of the mantle pyrope, ferropericlase, and perovskite lead us to conclude that the observed extremely high QS values of pyrope and perovskite at high P-T are a result of the strong lattice site distortions.

ACKNOWLEDGMENTS

We acknowledge S. Speziale for constructive comments and discussions, J. Liu for experimental assistance, and N. Seymour for manuscript editing. J. F. Lin acknowledges supports from the US National Science Foundation (EAR-0838221 and EAR-1056670) and the Carnegie/DOE Alliance Center (CDAC). The synchrotron work of the study was performed at HPCAT (Sector 16) of the Advanced Photon Source (APS), Argonne National Laboratory. HPCAT is supported by CIW, CDAC, UNLV and LLNL through funding from DOE-NNSA, DOE-BES and NSF. APS is supported by DOE-BES, under Contract No. DE-AC02-06CH11357.

REFERENCES

Amthauer, G., Annersten, H., and Hafner, S.S. (1976) The Mössbauer spectrum of ^{57}Fe in silicate garnets. Zeitschrift für Kristallographie, 143, 14-55.

Armbruster, T., Geiger, C.A., and Lager, G.A. (1992) Single-crystal X-ray structure study of synthetic pyrope almandine garnets at 100 and 293 K. American Mineralogist, 77, 512-521.

Badro, J., Rueff, J-P., Vankó, G., Monaco, G., Fiquet, G., and Guyot, F. (2004) Electronic transitions in perovskite: Possible nonconvecting layers in the lower mantle. Science, 305, 383-386.

Bancroft, G.M., Maddock, A.G., and Burns, R.G. (1967) Applications of the Mössbauer effect to silicate mineralogy-I. Iron silicates of known crystal structure. Geochimica et Cosmochimica Acta, 31, 2219-2246.

Bancroft, G.M. (1973) Mössbauer Spectroscopy: An Introduction for Inorganic Chemists and Geochemists, p. 252. Wiley, New York.

Bengtson, A., Li, J., and Morgan, D. (2009). Mössbauer modeling to interpret the spin state of iron in $(Mg, Fe)SiO_3$ perovskite. Geophysical Research Letters, 36, L15301.

Burns, R.G. and Solberg, T.C. (1988) ^{57}Fe-bearing oxide, silicate, and aluminosilicate minerals. In L.M. Coyne, F. Blake, S.W.S. McKeever, Eds., Spectroscopic Characterization of Minerals and Their Surfaces, ACS Symposium Series, 415, p263-283. American Chemical Society, Washington D.C.

Burns, R.G. (1993) Mineralogical application of crystal field theory. p527, Cambridge Univeristy Press, U. K.

Caracas, R., Mainprice, D., and Thomas, C. (2010) Is the spin transition in Fe^{2+}-bearing perovskite visible in seismology. Geophysical Research Letters, 37, L13309.

Chai, M. and Brown, J.M. (1997) The elastic constants of a pyrope-grossular-almandine garnet to 20 GPa. Geophysical Research Letters, 24, 523-526.

Černá, K., Mašláň, M., and Martinec, P. (2000) Mössbauer spectroscopy of garnets of almandine-pyrope series. Materials Structure, 7, 6-9.

Conrad, P.G., Zha, C-S., Mao, H-K., and Hemley, R.J. (1999) The high-pressure, single-crystal elasticity of pyrope, grossular and andradite. American Mineralogist, 84, 374-383.

Deer, W.R., Howie, R.A., and Zussman, J. (1982) An Introduction to the Rock-Forming Minerals, 696 p. Longman, White Plains, New York.

Dodokin, A.P., Lyubutin, I.S., Mill, B.V., and Peshkov, V.P. (1973) Mössbauer effect in antiferromagnetic substances with garnet structures. Soviet Journal of Experimental and Theoretical Physics, 36, 526-530.

Dyar, M.D., Agresti, D.G., Schaefer, M.W., Grant, C.A., and Sklute, E.C. (2006) Mössbauer spectroscopy of Earth and Planetary Materials. Annual Review of Earth and Planetary Sciences, 34, 83-125.

Haselton, H.T. Jr. and Westrum, E.F. Jr. (1980) Low-temperature heat capacities of synthetic pyrope, grossular, and $pyrope_{60}grossular_{40}$. Geochimica et Cosmochimica Acta, 44, 701-709.

Hazony, Y. and Axtmann, R.C. (1971) On QS-IS correlations in iron compound. Chemical Physics Letters, 8, 571–573.

Huggins, F.E. (1975) The 3*d* levels of ferrous ions in silicate garnets. American Mineralogist, 60, 316-319.

Hsu, H., Umemoto, K., Blaha, P., and Wentzcovitch, R.M. (2010) Spin states and hyperfine interactions of iron in (Mg, Fe)SiO_3 perovskite under pressure. Earth and Planetary Science Letters, 294, 19–26.

Hsu, H., Blaha, P., Cococcioni, M., and Wentzcovitch, R.M. (2011) Spin-state crossover and hyperfine interactions of ferric iron in $MgSiO_3$ perovskite. Physical Review Letters, 106, 118501.

Geiger, C.A., Armbruster, T., Lager, G.A., Jiang, K., Lottermoser, W., and Amthauer, G. (1992) A combined temperature dependent ^{57}Fe Mössbauer and single crystal X-ray diffraction study of synthetic almandine: Evidence for the Gol'danskii-Karyagin Effect. Physics and Chemistry of Minerals, 19, 131-126.

Gibbs, G.V. and Smith, J.V. (1965) Refinement of the crystal structure of synthetic pyrope. American Mineralogist, 50, 2023-2039.

Goncharov, A.F., Struzhkin, V.V., and Jacobsen, S.D. (2006) Reduced radiative conductivity of low-spin (Mg,Fe)O in the lower mantle. Science, 312, 1205-1208.

Goto, T., Ahrens, T.J., Rossman, G.R., and Syono, Y. (1980) Absorption spectrum of shock-compressed Fe^{2+}-bearing MgO and the radiative conductivity of the lower mantle. Physics of the Earth and Planetary Interiors, 22, 277-288.

Ingalls, R. (1964) Electric-field gradient tensor in ferrous compounds. Physical Review, 133, 787-795.

Jackson, J.M., Sturhahn, W., Shen, G., Zhao, J., Hu, M.Y., Errandonea, D., Bass, J.D., and Fei, Y. (2005) A synchrotron Mössbauer spectroscopy study of (Mg,Fe)SiO_3 perovskite up to 120 GPa. American Mineralogist, 90, 199-205.

Jiang, F., Speziale, S., and Duffy, T. S. (2004) Single-crystal elasticity of grossular- and almandine-rich garnets to 11 GPa by Brillouin scattering, Journal of Geophysical Research, 109, B10210, doi: 10.1029/2004JB003081.

Kantor, I.Y., Dubrovinsky, L.S., and McCammon, C.A. (2006) Spin crossover in (Mg,Fe)O: A Mössbauer effect study with and alternative interpretation of x-ray emission spectroscopy data. Physical Review B, 73, 100101(R).

Keppler, H., McCammon, C.A., and Rubie, D.C. (1994) Crystal field and charge transfer spectra of (Mg,Fe)SiO_3 perovskite. American Mineralogy, 79, 1215-1218.

Keppler, H., Kantor, I., and Dubrovinsky, L.S. (2007) Optical absorption spectra of ferropericlase to 84 GPa. American Mineralogist, 92, 433-436.

Li, J., Sturhahn, W., Jackson, J.M., Struzhkin, V.V., Lin, J.F., Zhao, J., Mao, H-K., and Shen, G. (2006) Pressure effect on the electronic structure of iron in (Mg,Fe)(Si,Al)O_3 perovskite: a combined synchrotron Mössbauer and X-ray emission spectroscopy study up to 100 GPa. Physics and Chemistry of Minerals, 33, 575-585.

Lin, J.F., Gavriliuk, A.G., Struzhkin, V.V., Jacobsen, S.D., Sturhahn, W., Hu, M.Y., Chow, P., and Yoo, C. S. (2006) Pressure-induced electronic spin transition of iron in magnesiowüstite-(Mg,Fe)O. Physical Review B, 73, 113107.

Lin, J.F., Watson, H., Vankó, G., Alp, E.E., Prakapenka, V.B., Dera, P., Struzhkin, V.V., Kubo, A., Zhao, J., McCammon, C., and Evans, W.J. (2008) Intermediate-spin ferrous iron in lowermost mantle post-perovskite and perovskite. Nature Geosciences, 1, 688-891.

Lin, J.F., Gavriliuk, A.G., Sturhahn, W., Jacobsen, S.D., Zhao, J., Lerche, M., and Hu, M. (2009) Synchrotron Mössbauer spectroscopic study of ferropericlase at high pressures and temperatures. American Mineralogist, 94, 594–599.

Lin, J.F., Mao, Z., Jarrige, I., Xiao, Y., Chow, P., Okuchi, T., Hiraoka, N., and Jacobsen, S.D. (2010) Resonant X-ray emission study of the lower-mantle ferropericlase at high pressures. American Mineralogist, 95, 1125-1131.

Lin, J.F., Alp, E.E., Mao, Z., Inoue, T., McCammon, C., Xiao, Y., Chow, P., and Zhao, J. (2012) Electronic spin and valence states of iron in the lower-mantle silicate perovskite by synchrotron Mössbauer spectroscopy. American Mineralogist, 97, 592-597.

Lyubutin, I.S. and Dodokin, A.P. (1970) Temperature dependence of the Mössbauer effect for Fe^{2+} in dodecahedral coordination in garnet. Kristallografiya, 15, 1249-1250.

Mao, H-K., Xu, J., and Bell, P.M. (1986) Calibration of the ruby pressure gauge to 800 kbar under quasihydrostatic conditions. Journal of Geophysical Research, 91, 4673-4676.

Mao Z., Lin, J.F., Jacobs, C., Watson, H.C., Xiao, Y., Chow, P., Alp, E.E., and Prakapenka, V.B. (2010) Electronic spin and valence states of Fe in $CaIrO_3$-type silicate post-perovskite in the Earth's lowermost mantle.

Mao. Z., Lin, J.F., Scott, H.P., Watson, H.C., Prakapenka, V.B., Xiao, Y., Chow, P., and McCammon, C. (2011) Iron-rich perovskite in the Earth's lower mantle. Earth and Planetary Science Letters, 309, 179-184.

McCammon, C., Kantor, I., Narygina, O., Rouquette, J., Ponkratz, U., Sergueev, I., Mezouar, M., Prakapenka, V., and Dubrovinsky, L.S. (2008) Intermediate-spin ferrous iron in lower mantle perovskite. Nature Geoscience, 1, 684–687.

McCammon, C., Dubrovinsky, L., Narygina, O., Kantor, I., Wu, X., Glazyrin, K., Sergueev, I., and Chumakov, A.I. (2010) Low-spin $^{Fe2+}$ in silicate perovskite and a possible layer at the base of the lower mantle. Physics of the Earth and Planetary Interiors, 180, 215-221.

Murad, E. and Wagner, F.E. (1987) The Mössbauer spectrum of almandine. Physics and Chemistry of Minerals, 14, 264-269

Narygina, O., Mattesini, M., Kantor, I., Pascarelli, S., Wu, X., Aquilanti, G., McCammon, C., and Dubrovinsky, L.S. (2009) High-pressure experimental and computational XANES studies of $(Mg,Fe)(Si,Al)O_3$ perovskite and (Mg,Fe)O ferropericlase as in the Earth's lower mantle. Physical Review B, 79, 174115.

Narygina, O.V., Kantor, I.Y., McCammon, C.A., and Dubrovinsky, L.S. (2010) Electronic state of Fe^{2+} in $(Mg,Fe)(Si,Al)O_3$ perovskite and $(Mg,Fe)SiO_3$ majorite at pressures up to 81 GPa and temperatures up to 800 K. Physics and Chemistry of Minerals, 37, 407-415.

Prandl, W. (1971) Die magnetische Struktur und die Atomparameter des Almandins $Al_2Fe_3(SiO_4)_3$. Zeitschrift für Kristallographie, 134, 333-343.

Rekhi, S., Dubrovinsky, L., and Saxena, S. (1999) Temperature-induced ruby fluorescence shifts up to a pressure of 15 GPa in an externally heated diamond anvil cell. High Temperatures-High Pressures, 31, 299-305.

Ringwood, A.E. (1991) Phase transformations and their bearing on the constitution and dynamics of the mantle. Geochimica et Cosmochimica Acta, 55, 2083-2110.

Sinogeikin, S.V. and Bass, J.D. (2000) Single-crystal elasticity of pyrope and MgO to 20 GPa by Brillouin scattering in the diamond anvil cell. Physics of the Earth and Planetary Interiors, 120, 43-62.

Stackhouse, S., Brodholt, J.P., Dobson, D.P., and Price, G.D. (2006), Electronic spin transitions and the seismic properties of ferrous iron bearing $MgSiO_3$ post-perovskite.

Geophysical Research Letters, 33, L12S03.

Sturhahn, W. (2000) CONUSS and PHOENIX: Evaluation of nuclear resonant scattering data. Hyperfine Interactions, 125, 149–172.

Umemoto, K., Hsu, H., and Wentzcovitch, R.M. (2010) Effect of site degeneracies on the spin crossovers in (Mg,Fe)SiO_3 pervoskite. Physics of the Earth and Planetary Interiors, 180, 109-124.

Wang, L., Essene, E.J., and Zhang, Y. (2000) Direct observation of immiscibility in pyrope-almandine-grossular garnet. American Mineralogist, 85, 41-46.

White, W.B. and Moore, R.K. (1972) Interpretation of the spin-allowed bands of Fe^{2+} in silicate garnets. American Mineralogist, 57, 1692-1710.

Yu Y.G., Hsu, H., Cococcioni, M., and Wentzcovitch, R.M. (2012) Spin states and hyperfine interactions of iron incorporated in $MgSiO_3$ post-perovskite. Earth and Planetary Science Letters, 331-332, 2012.

Zemann, A. and Zemann, J. (1961) Verfeinerung der kristallstruktur von synthetischem pyrope, $Mg_3Al_2(SiO_4)_3$. Acta Crystallographica, 14, 835-837.

Zhang, F. and Oganov, A.R. (2006) Valence state and spin transitions of iron in Earth's mantle silicates. Earth and Planet Science Letters, 249, 436-443.

Figure Captions:

Figure 1. Crystal-field splitting and stabilization energy of Fe^{2+}-bearing pyrope, silicate perovskite, and ferropericlase. Three different crystal-field models are shown: (a) free ion; (b) undistorted field; (c) distorted site. CFSE: crystal-field stabilization energy; Δ_C: crystal-field splitting energy; Δ: energy separation between the lowest d_{xy} and d_{z^2} levels of the e_g states in a distorted dodecahedral site of the high-spin Fe^{2+} in pyrope and perovskite, or between the lowest d_{xy} and upper d_{xz} and d_{zy} levels of the t_{2g} states in a distorted octahedral Fe^{2+} site in ferropericlase. Literature values shown here are taken for pyrope from Huggins (1975), for silicate perovskite [$(Mg_{0.94}Fe_{0.06})SiO_3$] from Keppler et al. (1994), and for ferropericlase (up to 25% Fe in [(Mg,Fe]O]) from Bancroft (1973), Burns (1985, 1993), Goto (1980), Goncharov et al. (2006), Keppler et al. (2007), and Lin et al. (2009).

Figure 2. Representative synchrotron Mössbauer spectra of Fe-bearing pyrope [$(Mg_{0.8}Fe_{0.2})_3Al_2Si_3O_{12}$] at high pressures and/or temperatures. (a). Ambient pressure and high temperatures; (b). 25 GPa and high temperatures. (c). Mössbauer spectra of the sample with stainless steel as an external reference at 25 GPa and high temperatures. Red circles: measured spectrum; black lines: modeled results using CONUSS program (Sturhahn et al. 2000).

Figure 3. Quadrupole splitting (QS) and chemical shift (CS) of Fe-bearing pyrope at high pressures and 300 K. Solid circles: $(Mg_{0.8}Fe_{0.2})_3Al_2Si_3O_{12}$ (py80alm20); solid diamonds: $Fe_3Al_2Si_3O_{12}$ (alm100). Solid lines represent the trend of the QS and CS as a function of

pressure. Standard deviations of QS and CS as derived the systematic analyses of the modeling are approximately ±0.005 mm/s, respectively, showed at the bottom (top) right corner of the QS (CS) plot. The CS values shown have been converted to the values with respect to α-Fe reference.

Figure 4. Quadrupole splitting (QS) and chemical shift (CS) of Fe-bearing pyrope ($(Mg_{0.8}Fe_{0.2})_3Al_2Si_3O_{12}$)) at high pressures and temperatures. Solid circles: derived experimental values. Solid curves in (a) represent calculated QS using the model by Huggins (1975), whereas lines in (b) are a guide to the eye and highlight the linar temperature dependence of CS. The standard deviations of the QS and CS values are shown as ±1σ at the top right corner of the figure.

Figure 5. Derived QS(0K) and lattice contribution (QS_{latt}) of Fe-bearing pyrope ($(Mg_{0.8}Fe_{0.2})_3Al_2Si_3O_{12}$) at high pressures. (a). QS(0K) and QS_{latt} contributions of the QS; (b). Ratio of the QS_{latt} contribution to the total QS as a function of pressure. Representative error bars are shown as ±1σ at the bottom right corner (a) for the QS(0K) and QS_{latt} contributions, and at the bottom right corner (b) for the ratio of the QS_{latt} contribution to the total QS.

Figure 6. Energy separation (Δ) of the two lowest energy levels of Fe-bearing pyrope [$(Mg_{0.8}Fe_{0.2})_3Al_2Si_3O_{12}$] at high pressures. (a). Derived Δ of Fe^{2+} in the dodecahedral site; (b). Variation of the energy separation in percentage with respect to the value at ambient pressure (Δ_0). Representative error bars are shown as ±1σ at the top right corner of the

figure. Detailed crystal-field splitting diagram and energy of the Fe^{2+}-bearing pyrope are shown in Fig. 1.

Figure 7. Quadrupole splitting (QS) of Fe^{2+} in Fe-bearing pyrope compared with other phases. Literature values for perovskite (Pv) from Jackson et al. (2005), Li et al. (2006), McCammon et al. (2008), Lin et al. (2008) (2012), Hsu et al. (2010, 2011), Narygina et al. (2010), and Mao et al. (2011); for post-perovskite (Ppv) from Lin et al. (2008), Mao et al. (2010), and Yu et al. (2012); for ferropericlase (fp) from Kantor et al. (2006), and Lin et al. (2006, 2009).

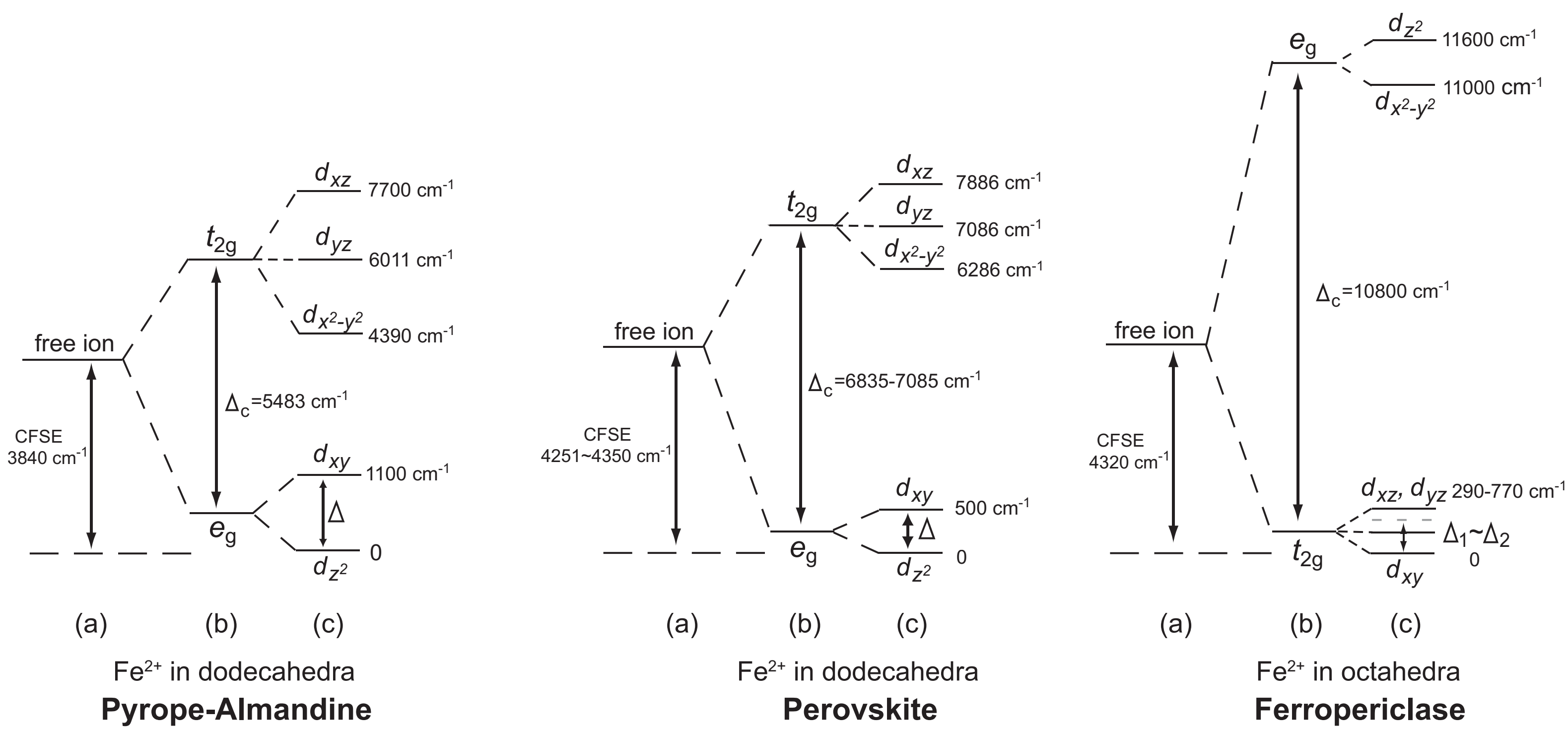
free ion
CFSE
3840 cm-1
t2g
eg
Δc=5483 cm-1
dxz 7700 cm-1
dyz 6011 cm-1
dx2-y2 4390 cm-1
dxy 1100 cm-1
Δ
dz2 0
(a) (b) (c)
Fe2+ in dodecahedra
Pyrope-Almandine
free ion
CFSE
4251~4350 cm-1
t2g
eg
Δc=6835-7085 cm-1
dxz 7886 cm-1
dyz 7086 cm-1
dx2-y2 6286 cm-1
dxy 500 cm-1
Δ
dz2 0
(a) (b) (c)
Fe2+ in dodecahedra
Perovskite
free ion
CFSE
4320 cm-1
eg
t2g
Δc=10800 cm-1
dz2 11600 cm-1
dx2-y2 11000 cm-1
dxz, dyz 290-770 cm-1
Δ1~Δ2
dxy 0
(a) (b) (c)
Fe2+ in octahedra
Ferropericlase

Figure 1

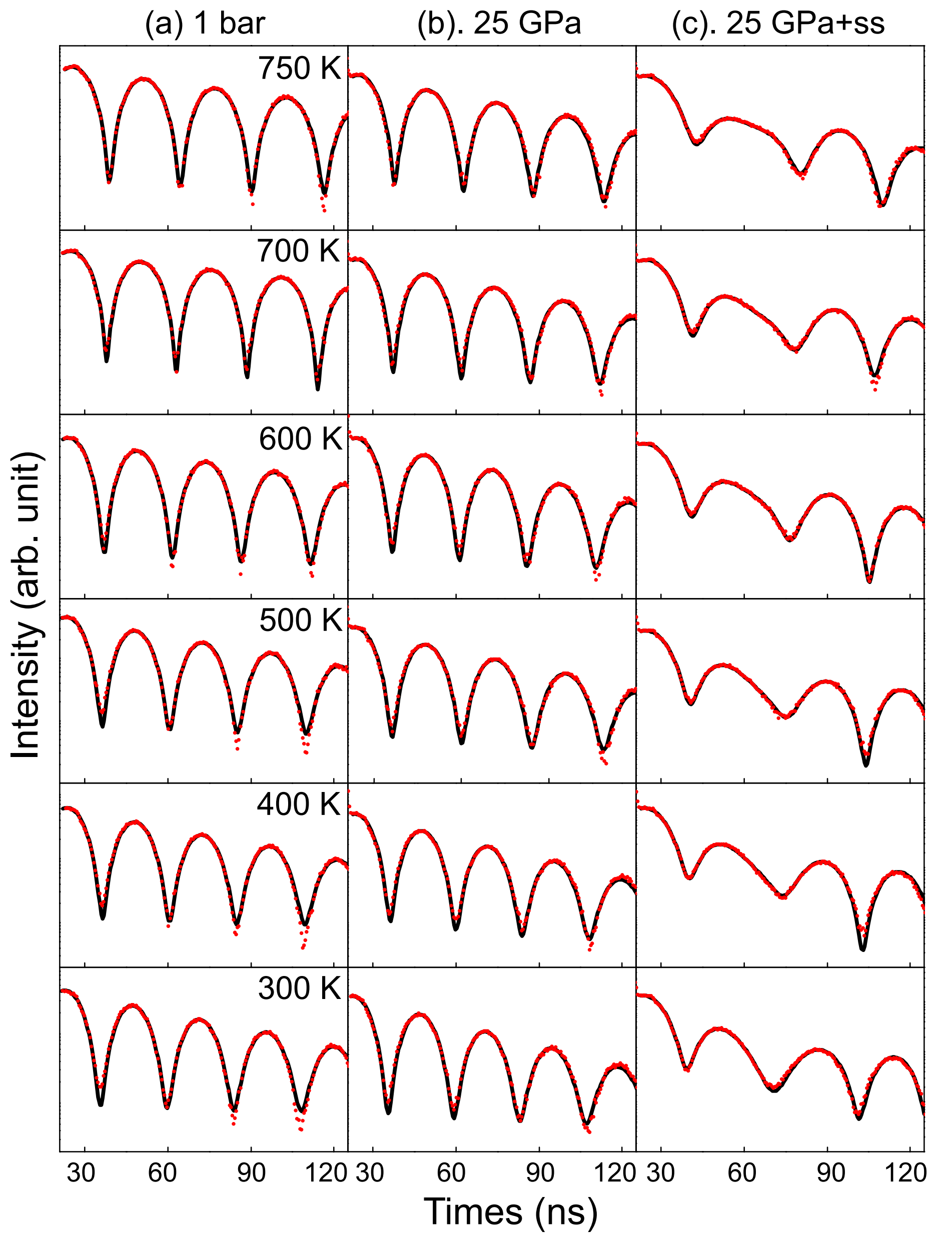
(a) 1 bar
(b). 25 GPa
(c). 25 GPa+ss
750 K
700 K
600 K
500 K
400 K
300 K
Intensity (arb. unit)
30
60
90
120
Times (ns)

Figure 2

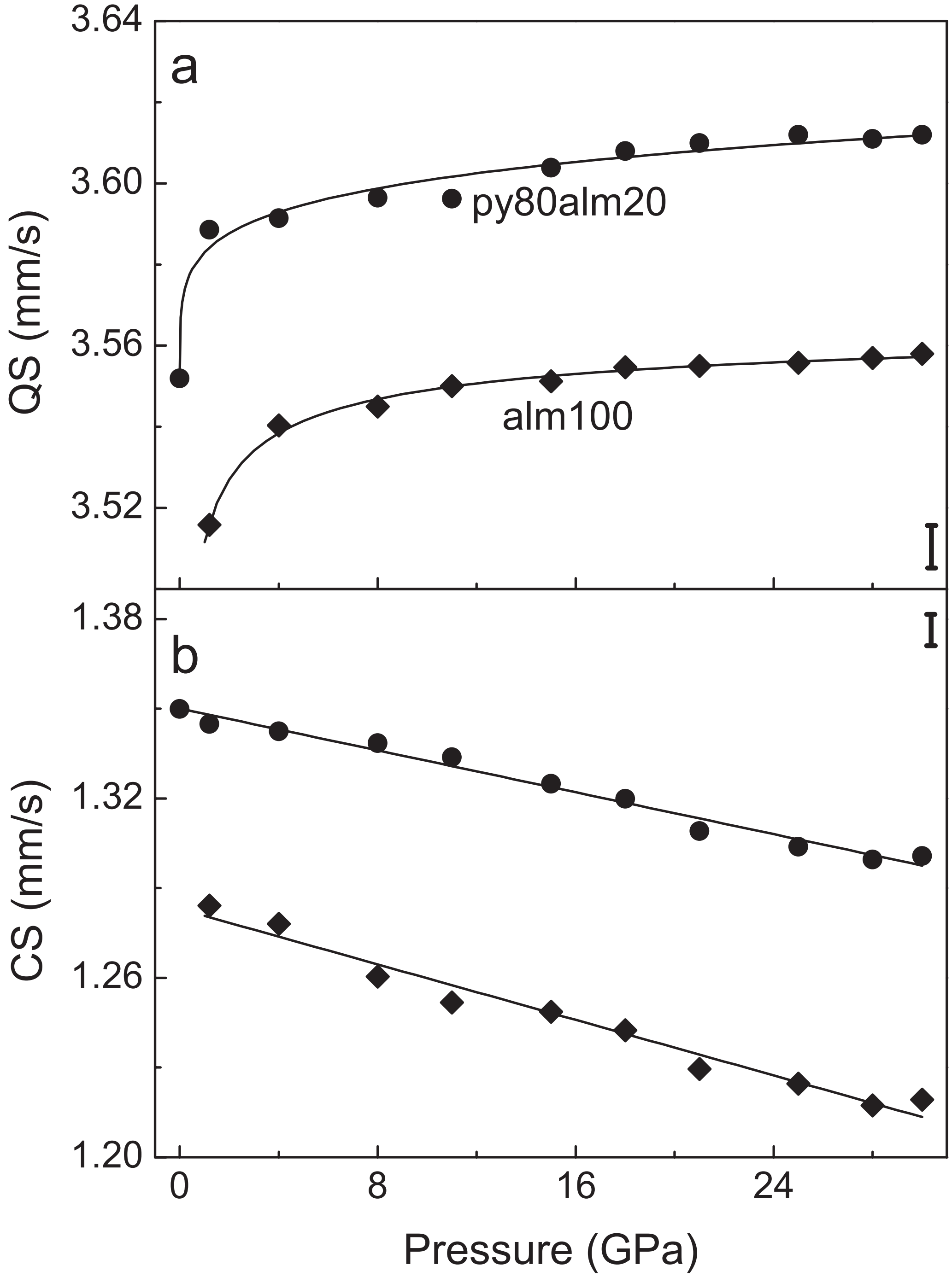
3.64
3.60
3.56
3.52
QS (mm/s)
a
py80alm20
alm100
1.38
1.32
1.26
1.20
CS (mm/s)
b
0
8
16
24
Pressure (GPa)

Figure 3

This is a preprint, the final version is subject to change, of the American Mineralogist (MSA)
Cite as Authors (Year) Title. American Mineralogist, in press.
(DOI will not work until issue is live.) DOI: http://dx.doi.org/10.2138/am.2013.4321

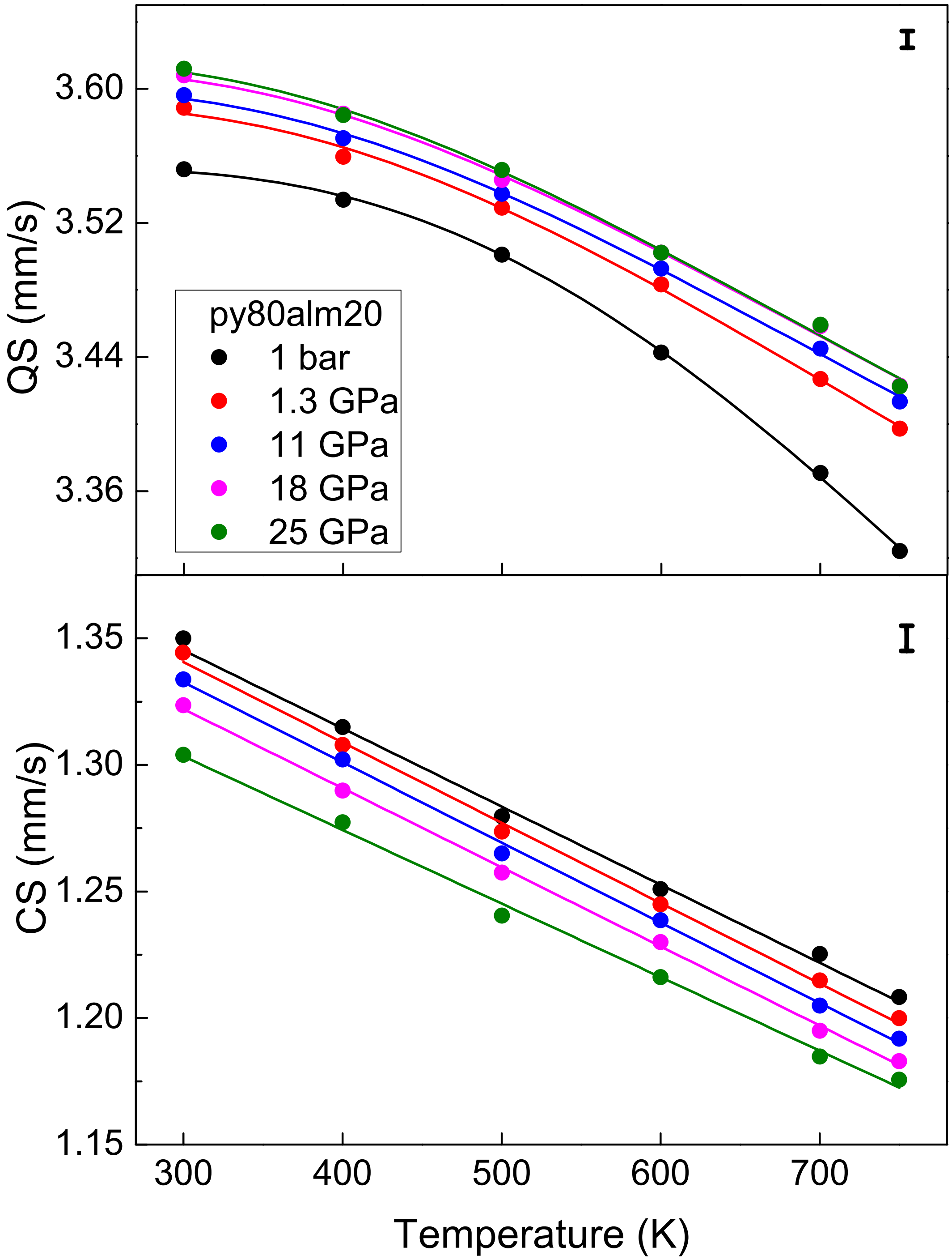

Figure 4

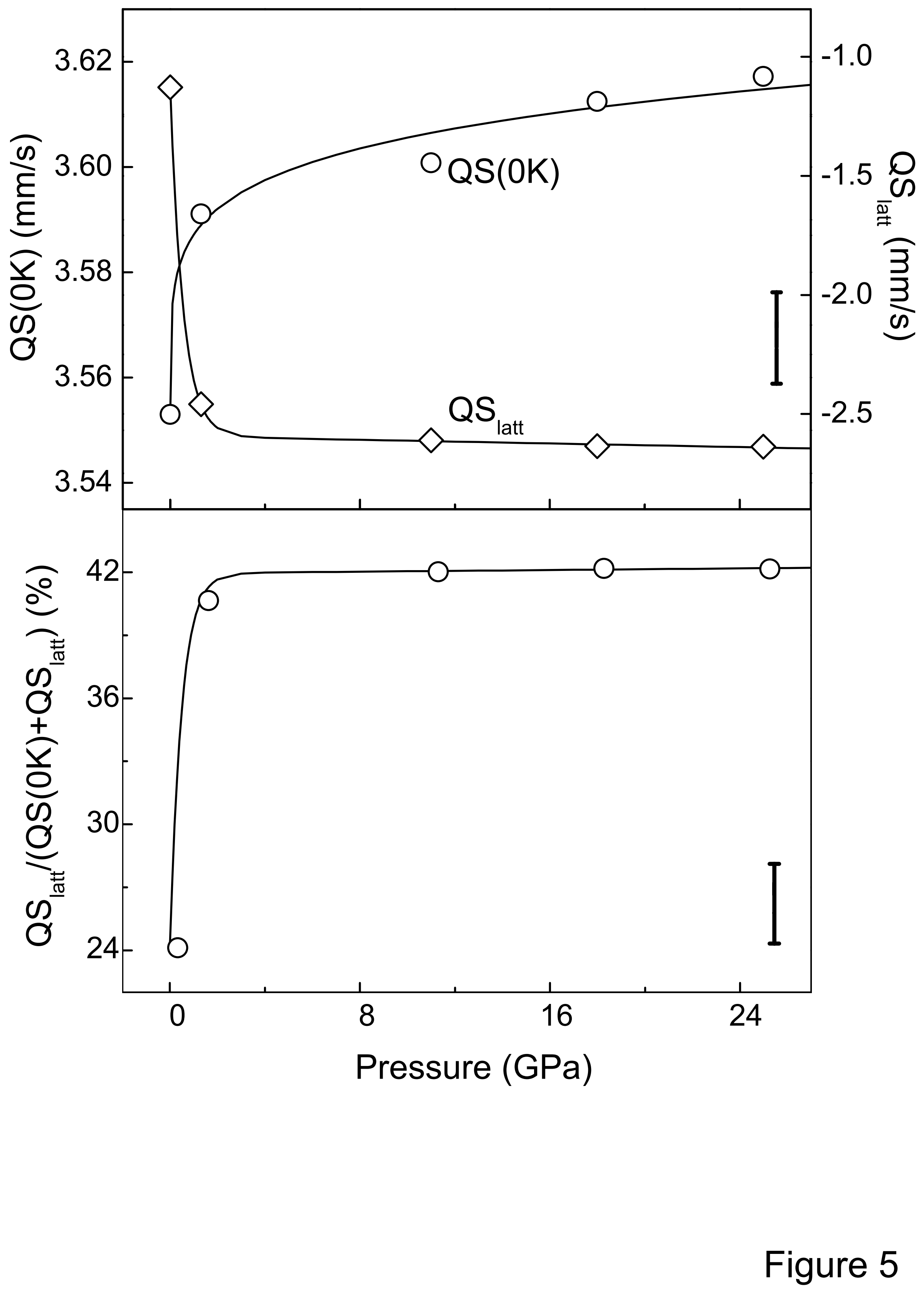
3.62
3.60
3.58
3.56
3.54
QS(0K) (mm/s)
QS(0K)
QS_{latt}
-1.0
-1.5
-2.0
-2.5
QS_{latt} (mm/s)
42
36
30
24
$QS_{latt}/(QS(0K)+QS_{latt})$ (%)
0
8
16
24
Pressure (GPa)

Figure 5

This is a preprint, the final version is subject to change, of the American Mineralogist (MSA)
Cite as Authors (Year) Title. American Mineralogist, in press.
(DOI will not work until issue is live.) DOI: http://dx.doi.org/10.2138/am.2013.4321

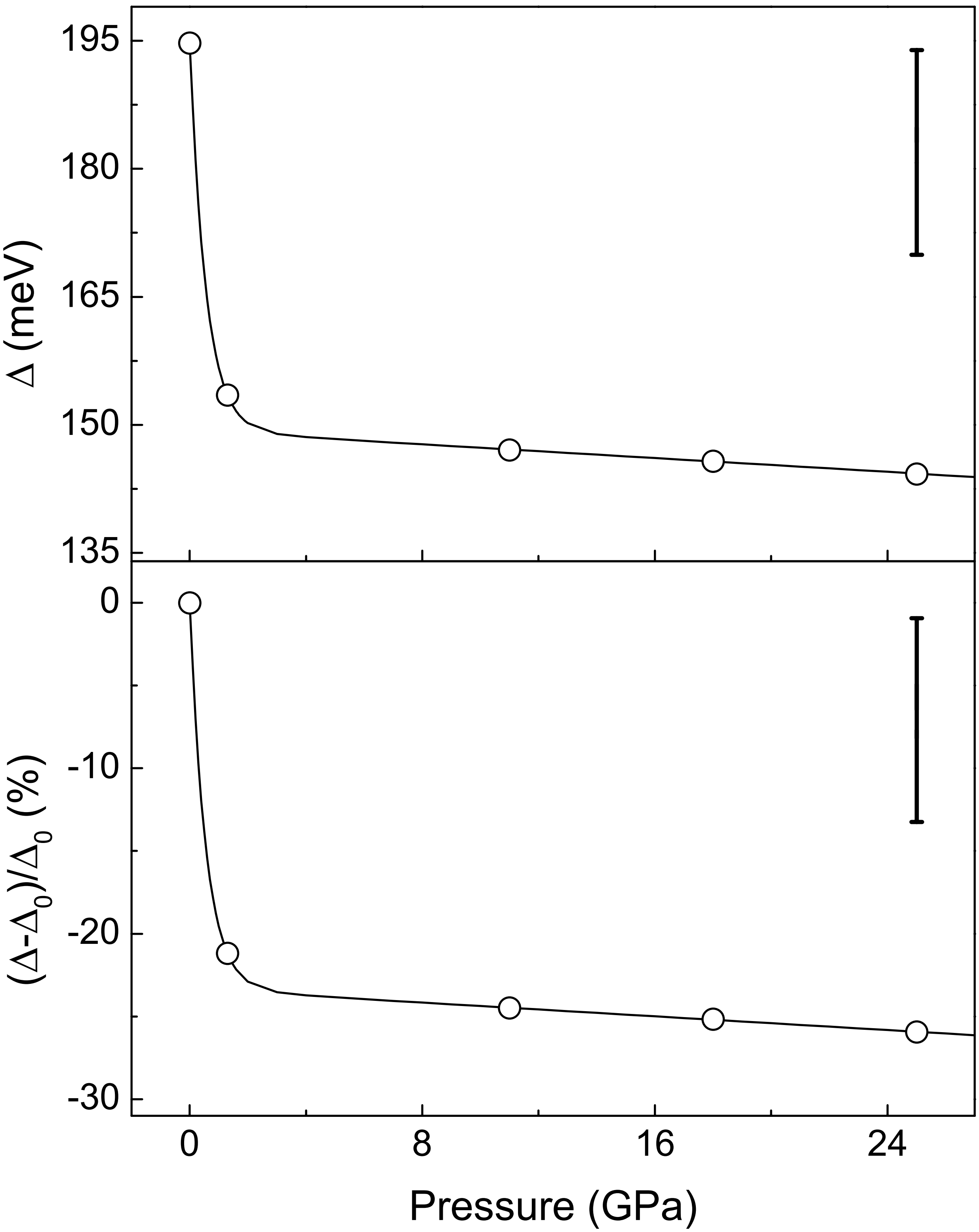

Figure 6

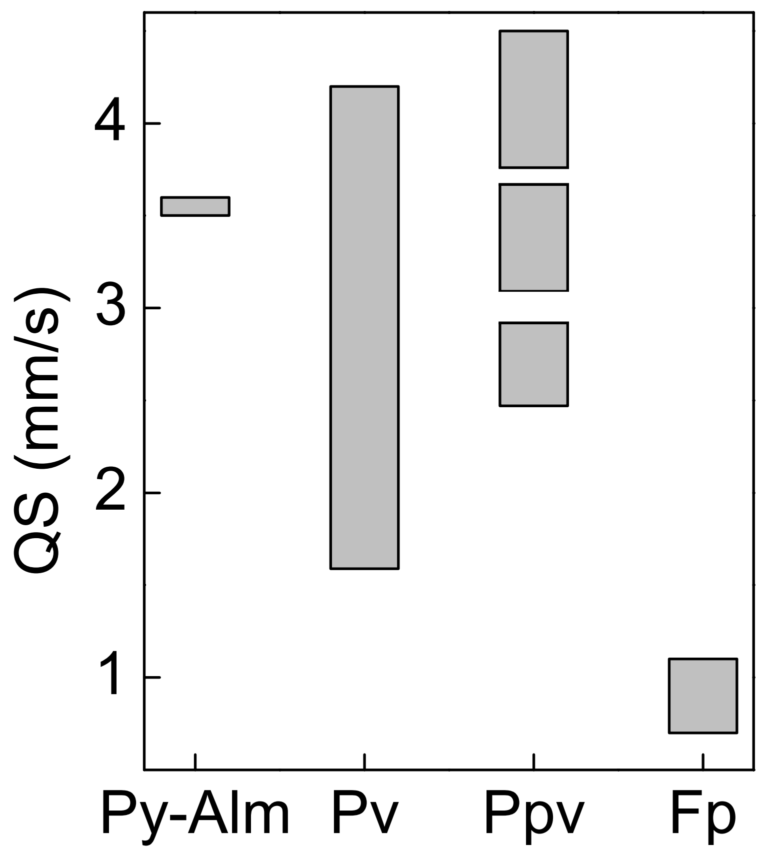

Figure 7